OXIDE THICKNESS MEASUREMENTS AND CHARACTERIZATION OF TWO Zr-2.5Nb PRESSURE TUBES OF EMBALSE NUCLEAR POWER PLANT

R. Bordoni, A.M. Olmedo*

Departamento Química de Reactores, Gerencia Química, Comisión Nacional de Energía Atómica. Avda Gral Paz 1499 (B1650KNA) San Martín, Buenos Aires; Argentina

*Corresponding Author, e-mail: olmedo@cnea.gov.ar.

Recibido: Agosto 2010. Aprobado: Enero 2011.
Publicado: Mayo 2011.

ABSTRACT
Embalse Nuclear Power Plant (CNE) is a PHWR (Pressurized Heavy Water Reactor), CANDU 600, with Pressure Tubes (PT) of Zr-2.5Nb. Two PTs were removed from this plant after 9.9 effective full power years (EFPY), one of the central zone and the other of the peripheric one of the core. Samples cut out from these PTs allowed the oxide film characterization from the inside (internal side) and outside (external side) surfaces of the PTs and to measure also the oxide thickness. The inside oxide thickness varies between 6 to 12 μm along the peripheric pressure tube, and between 7 to 15 μm along the central tube. The maximum average corrosion rate was 1.2 μm/EFPY and 1.5 μm/EFPY at the outlet end of the peripheric and central tubes respectively, that are within the range of the values reported for PTs removed in other CANDU reactors. The outside oxide thickness varies between 2 to 5 μm and 2 to 3.5 μm for the peripheric and central tubes respectively.

Keywords: corrosion, high T, pressure tube, Zr-2.5Nb.

MEDICIÓN DEL ESPESOR Y CARACTERIZACIÓN DEL ÓXIDO DE DOS TUBOS DE PRESIÓN EXTRAÍDOS DE LA CENTRAL NUCLEAR DE EMBALSE

RESUMEN
La Central Nuclear de Embalse (CNE) es una Central Nuclear refrigerada por agua pesada presurizada, CANDU 600, con tubos de presión (TPs) de Zr-2.5Nb. Después de 9,9 años de plena potencia (APP), se extrajeron dos TPs, uno de la zona central del núcleo y el otro de la zona periférica. Se cortaron probetas de ambos PTs para caracterizar las superficies interna y externa de los mismos y también para medir el espesor del óxido crecido sobre ellas. El espesor del óxido interno varió entre 6 y 12 μm a lo largo del tubo periférico y entre 7 y 15 μm a lo largo del tubo central.. La velocidad de corrosión máxima fue de 1.2 μm/APP y de 1.5 μm/APP en el extremo de salida del tubo periférico y del tubo central respectivamente, valores que son similares a los informados para TPs extraídos de otras centrales CANDU. El espesor del óxido externo varió entre 2 y 5 μm a lo largo del tubo periférico y entre 2 y 3.5 μm a lo largo del tubo central.

Palabras claves: corrosión, alta T, tubo de presión, Zr-2.5Nb.

INTRODUCTION

In a previous work [1] we have emphasized the importance of the use of techniques like Scanning Electron Microscopy (SEM) and EDS (Energy Dispersive Spectroscopy) as powerful and effective tools to evaluate the effect of the environment in the structural materials of either in conventional or nuclear power plants, particularly related with corrosion, i.e. the growth of oxides and deposits grown on the materials due to their interaction with the coolant.

The CANDU reactor consists of a large tank (calandria), containing heavy water moderator at 70ºC, that is penetrated by about 400 fuel channel arranged in a regular lattice. Each channel consists of a pressure tube (PT), containing natural uranium fuel and heat transport heavy water at a pressure of around 10 Mpa and temperature ranging from 250 to 300ºC, surrounded and insulated from the cold moderator, by a calandria tube.

The space between the pressure and calandria tubes contains dry carbon dioxide and is called the gas annulus. The internal side of the PT is in contact with heavy water and the external side of it contacts with carbon dioxide.

The PTs of CANDU reactors are manufactured with Zr-2.5%Nb alloy. These tubes are extruded at around 820 to 850°C, cold worked 20 to 30% and stress relieved (autoclaved) in steam at 400°C. At the extrusion temperature, the tube microstructure consists of about 80% of beta zirconium (β-Zr) and 20% of alpha zirconium (α-Zr). During air cooling after the extrusion, the β-Zr transforms to α-Zr by growing on the existing elongated α-grains produced during the extrusion, while the β-Zr becomes progressively enriched in Nb. Finally, extruded tubes contain α-grains up to about 10 μm long, 1 μm wide and 0.5 μm thick which have a hcp structure containing approximately 0.6 to 1%wt Nb. These α-grains are surrounded by a grain boundary network of metastable β-Zr, with a bcc structure, that contains about 18 to 20% wt % Nb. Cold drawing causes and additional elongation of the α-grains and introduces a high density of dislocations [2,3]. A SEM micrograph of a PT microstructure is shown in the Figure 12 of a previous work [1].

The initial content of hydrogen of the tubes is very low, however when the lithiated heavy water coolant that flows through the inside surfaces of the Zr-2.5Nb pressure tubes (PTs), reacts with them to form zirconium oxide (ZrO_2) and deuterium. During this corrosion reaction, part of D_2 is released to the coolant but a small fraction of it, is absorbed by the material. During service, the equivalent hydrogen (hydrogen + deuterium) of PTs increases slowly due to the low corrosion rate of this alloy in the typical CANDU heat transport chemistry conditions of the primary coolant. The corrosion rate of Zr-2.5Nb depends on different variables like: temperature, coolant chemistry, fast neutron flux, fluence and material microstructure [4,5].

The stress relieved in steam at 400°C for 24 h induces some microstructure decomposition of Zr-2.5Nb and literature also reports that the metastable β-phase transforms into other phases with time at temperatures lower than 475°C producing a decomposition of the β-Zr phase in the following way [6]:

$$\beta\text{-Zr} \rightarrow \omega+\beta\text{-Zr}_{enr.} \rightarrow \alpha\text{-Zr}+\omega+\beta\text{-Zr}_{enr.} \rightarrow \alpha\text{-Zr}+\beta\text{-Zr}_{enr.} \rightarrow$$
$$\rightarrow \alpha\text{-Zr}+\beta\text{-Zr}_{enr.}+\beta\text{-Nb} \rightarrow \alpha\text{-Zr}+\beta\text{-Nb}$$

The autoclaving treatment at 400°C plus service in reactors at temperatures around 300°C will therefore transform the β- network, leading the microstructure of the PTs to a more nearly equilibrium one [7-10] thus increasing the corrosion resistance of the PTs alloy. The fast neutron flux (E> 1 Mev), also induces microstructure changes in the PTs material leading to a better corrosion behavior of PTs [11,12].

In order to know the in service corrosion behavior of PTs, it is necessary to characterize the oxide grown on their surfaces and also to measure the oxide thickness. The knowledge of how the corrosion behavior is modified by the influence of fluence during PTs service allow us to have a better understanding of the role of different variables (neutron flux, temperature and microstructure) on the corrosion behavior.

The purpose of this work was to characterize the oxides from the inside and outside surfaces of two PTs removed from Embalse NPP and also to measure their oxide thicknesses in different zones. The corrosion rate of the inside surface of the PTs will also be compared with the corrosion rate of coupons machined from pressure tubes that were inserted in the CNE autoclaves located out of core (out-of-flux) in the PHTS (Primary Coolant Heat Transport System)[13].

MATERIALS AND METHODS

Two pressure tubes were removed from Embalse NPP after 3610 EFPD (Effective Full Power Days) i.e. 9.9 EFPY (Effective Full Power Years). The positions of the fuel channels in the reactor were A-14 (peripheric) and L-12 (central). Both fuel channels have a very different location when the neutron flux is considered. Figure 1 depicts the fast neutron flux (E>1Mev) along axial distance of the tube and Figure 2 plots the profile temperature of the primary coolant versus the axial distance along the tube. These Figures indicate that while the temperature profile is similar for both channels, the fast neutron flux of the central channel is nearly twice than that of the peripheric one.

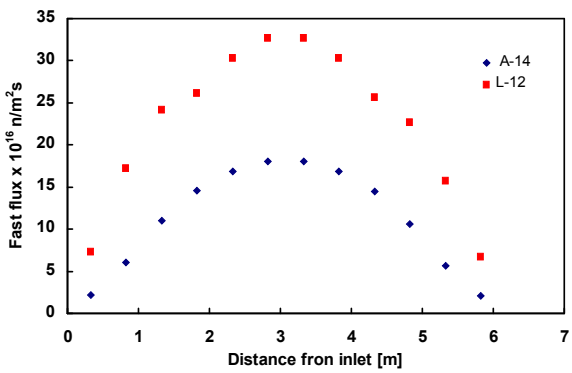

Fig. 1. Fast neutron flux axial profiles in fuel channels A-14 and L-12.

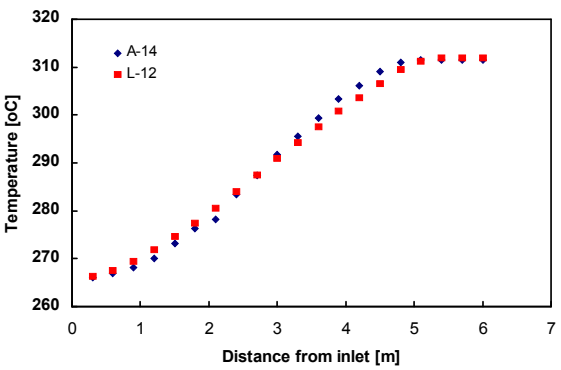

Fig. 2. Temperature axial profiles in fuel channels A-14 and L-12.

The chemical composition of the pressure tubes material is summarized in Table I, where it is indicated not only the principal constituents but also the impurities of the material.

Small specimens were cut out at 3, 6, 9 and 12 h o'clock positions from rings taken at 0.3, 3.1, 5.1 and 5.8 m axial locations from the inlet end of Embalse NPP Pressure Tubes. Using SEM the oxide thickness and the morphology characteristics of the inside and outside surfaces were studied. After machining and prior to the study, the specimens were decrudded in a solution of 50% (vol/vol) hydrochloric acid (HCl) at around 75°C during 3 h. Finally, the samples were rinsed in demineralized water, alcohol, acetone and after drying were stored in appropriate dryer. The samples were then cut approximately in two halves. One half was coated on both sides with a thin gold film in order to avoid any charging effect during the characterization of the surface oxide morphology. The other one was then mounted in an acrylic resin and grinded using SiC paper down to 1500 grit and finally polished with diamond paste up to 1 μm. These cross sections were then exposed to a mixture of 10% HF+15% HNO_3+35% H_2SO_4 in water, so that the metal was etched back in order to reveal the metal/oxide interface more clearly. Finally, these cross sections were also coated with a thin gold film in order to measure the oxide thickness of the inside and outside PTS surfaces.

Table I. Chemical composition of the Pressure Tube Material

Element	PT A-14	PT-L-12
Nb [%]	2.5	2.6
O [ppm]	960	1160
Al [ppm]	46	42
C [ppm]	110	110
Cr [ppm]	<80	<80
Fe [ppm]	385	699
Hf [ppm]	<40	<40
N [ppm]	32	53
Si [ppm]	49	<60
Zr	balance	balance

The oxide thickness on the inside surface of each sample was determined in the following way: for each sample 12

images were taken with SEM (using a magnification of around 1500 X), then 12 measurements with each image were taken. The average oxide thickness on each position (for each sample), results from the calculation of the average value of the collection of all the measurements taken at that position. The oxide thickness measurements in the spalling zones were not considered in the calculation. The same procedure was employed for the outside surfaces of both TPs.

RESULTS AND DISCUSSION

a. Oxide Morphology

The visual examination of the samples cut from the PTs showed that the inside surface of them were covered with an adherent black oxide. Figures 3 (a) and (b) show that the oxide morphology of PTs inside surface have topographical features typical of sandblast surfaces.

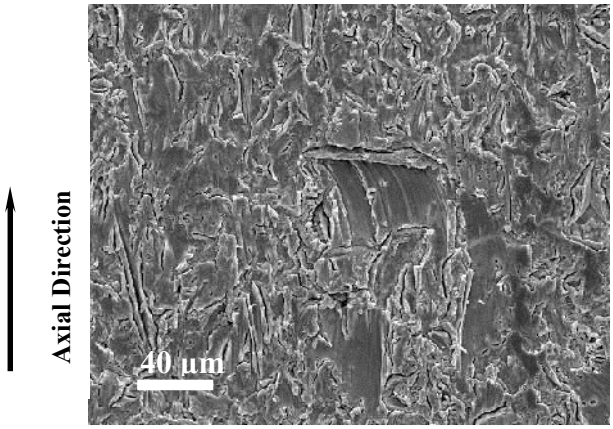

Fig. 3 (a). Typical oxide morphology of the inside surface. Sample taken at 12 o'clock, 0.3 m axial position from the inlet of PT A-14.

A representative oxide morphology of the inside surface of a sample at 6 o'clock location is shown in Figure 4. Figure 4 (a), presents clearly the axial scratches produced at the bottom of the tube during fueling caused by the fuel bundle bearing pads. The oxide morphology at the side zones of the scratch marks left by the bearing pads is similar to the oxide in others o'clock locations, Figure 4 (b). These scratch marks, are slight and innocuous. Warr and coworkers [12] reported similar oxide topographies and appearance of PTs removed from other CANDU plants.

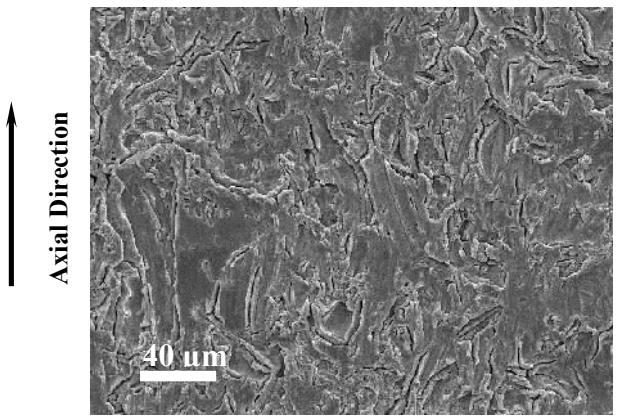

Fig. 3 (b). The same of Fig. 3(a) taken at 3 o'clock position.

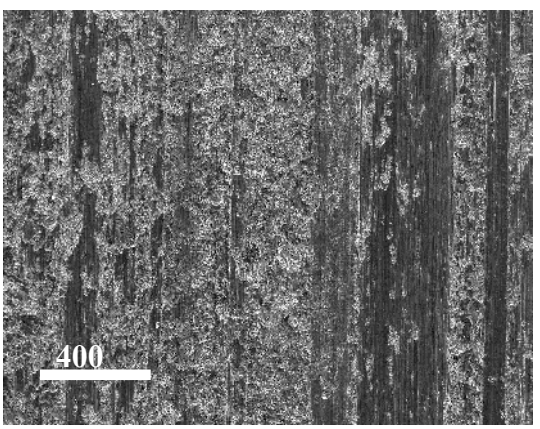

Fig. 4 (a) Typical oxide morphology of the inside surface taken at 6 o'clock, 0.3m axial position of PT A-14 showing fueling scratches

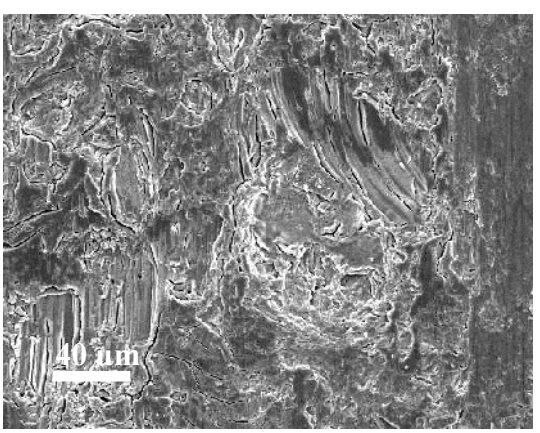

Fig. 4 (b) Magnification of Figure 5(a)

The inside surface oxide at other positions of both PTs presents a similar topography and appearance than those shown in Figures 3 and 4. A small number of spalling areas were observed in the first half part of the PTs, at 0.3 and 3.1 m axial locations. The density of spalling areas increases slightly in the second half of the tubes, at 5.1 and 5.8 m axial locations, being larger in the central fuel channel than in the peripheric one. These features can be seen in Figures 5 and 6.

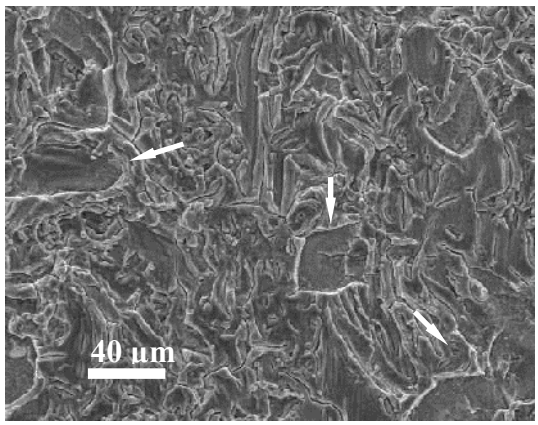

Fig. 5. Typical oxide morphology of the inside surfaces. Micrograph was taken at 12 o'clock and at 5.1 m from the inlet of PT A-14. Arrows indicate some spalling areas.

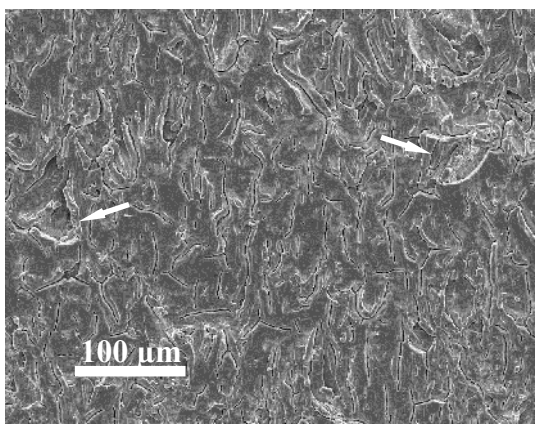

Fig. 6. Typical oxide morphology of the inside surfaces. Micrograph was taken at 12 o'clock and at 5.7 m from the inlet of PT L-12. Arrows indicate some spalling areas.

In all of the cross sections of the samples studied, neither the small spalling zones nor any other defect affect the protective character of the oxide film since in all the specimens, there was always at least 5-6 µm of adherent, compact and non damaged oxide at the oxide/metal interface. The protective character of oxide films that grow in zirconium alloys, in standard primary coolant chemistry, is due to the formation of a film composed of a compact, adherent internal layer at the oxide/metal interface of a thickness greater than 2-3 µm and a less dense, more porous external layer [7,12,14,16].

The visual appearance of the oxide on the outside surface was black, compact and was more reflective than that of the inside surface. Figure 7 shows a typical appearance of the outside surface oxide. This micrograph shows that the oxide film replicates the original outside tube surface. Small microcracks are also seen following the direction of the original grinding marks of the original external surface of the pressure tube. This is a common feature of the oxide of all PTs that do not affect the protective character of the oxide layer due to the small depth of these microcracks.

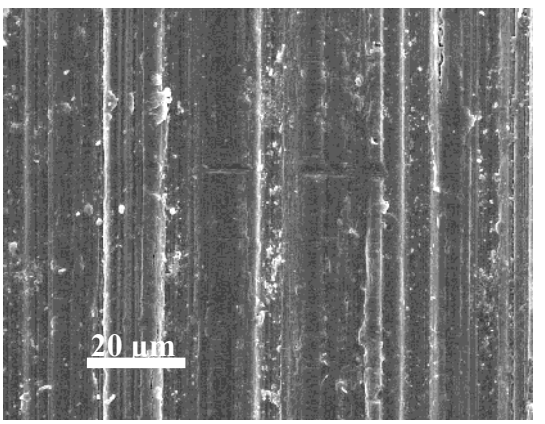

Fig. 7. Typical oxide morphology of the outside surface. This micrograph was obtained from a sample of PT L-12 at 12 o'clock and 5.8 m position from inlet.

3.b Oxide thickness and metallographic examinations

Figures 8 and 9 show the cross section micrographs of a sample at 12 o'clock located at 0.3 m position and at 6 o'clock located at 5.8 m position from the inlet of the peripheric and central PTs respectively. The micrographs show that the oxide edge corresponding to the oxide/coolant interface is very irregular in accordance with the oxide morphology showed in Figures 3, 4 and 5.

These two oxide cross sections are very similar to those reported in reference [12].

The cross section micrographs show a compact oxide layer with a few small microcracks perpendicular to the surface penetrating up to a distance smaller than half of oxide thickness. It can also be seen small areas of microspalling already mentioned, but the oxide non damaged and protective is always present at the metal/oxide interface. Other characteristic in these micrographs is the presence of lateral microcracks, that are typical of the zirconium oxide layers [7,14, 15, 16].

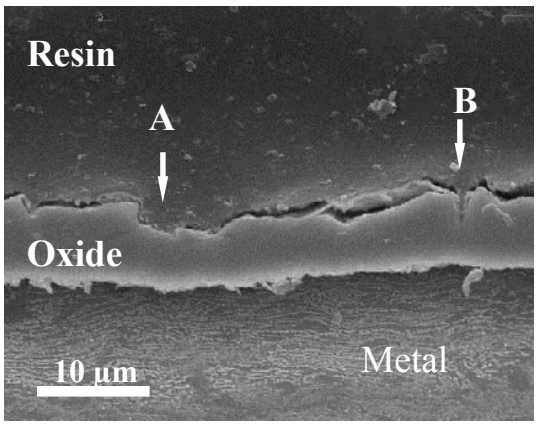

Fig. 8. Cross section of the inside surface sample from PT A-14 taken at 12 o'clock and 0.3 m position from the inlet.

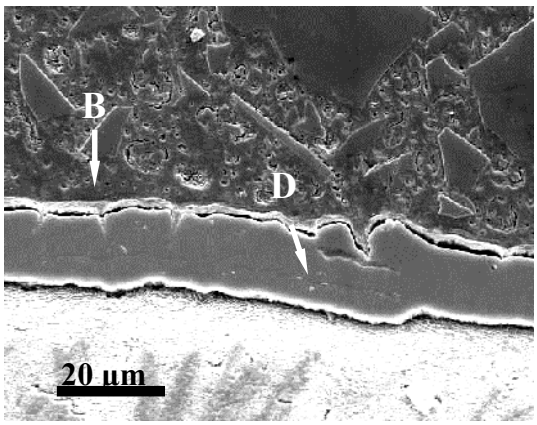

Fig. 9. Cross section of the inside surface sample from PT L-12 taken at 6 o'clock and 5.7m position from the inlet.

Arrow A indicates a small zone of spalling, arrows B show microcracks perpendicular to the surface and arrow D shows parallel microcracks.

Figures 10 and 11 show cross section micrographs of samples from the outside surface oxide. The differences in the aspect of the oxides shown in these two micrographs are a consequence that the samples were prepared in two different planes.

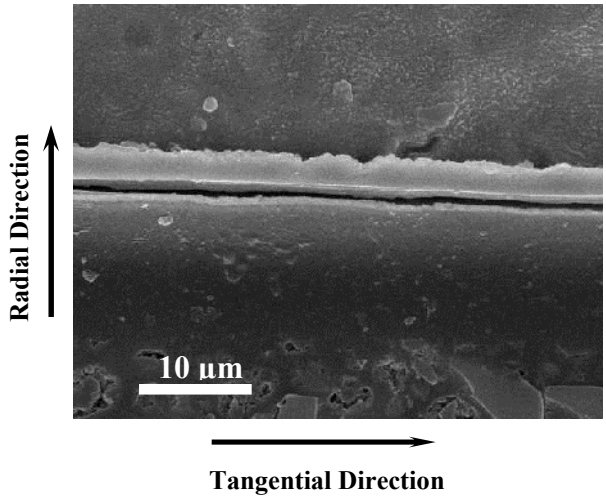

Fig.10. Cross section showing the external oxide appearance of PT A-14 taken at 12 o'clock and 5.8 m position from the inlet. The plane of the micrograph corresponds to a radial-tangential plane.

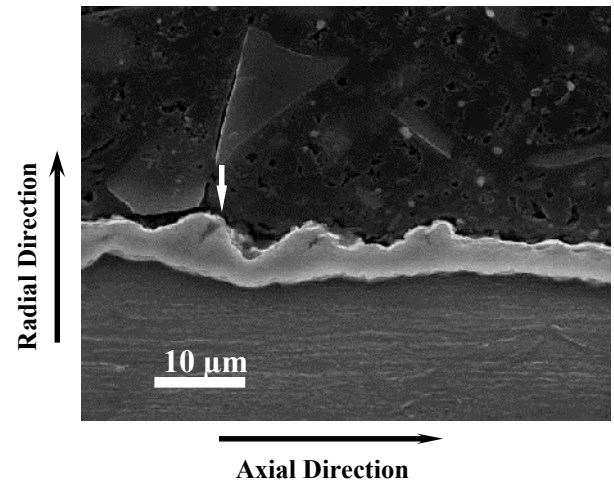

Fig. 11. Cross section showing the external oxide appearance of PT L-12 taken at 6 o'clock and 5.8 m position from the inlet. The plane of the micrograph corresponds to axial-radial plane.

Figure 10 shows the cross section on the radial-tangential plane that contains the original grinding marks of the PT, while Figure 11 shows the radial-axial plane that is perpendicular to the grinding marks. The orientation of the last cross section was prepared to analyze small defects that were seen in the morphological observations shown before. In Figure 10 no defects are seen and the oxide edge at the oxide/annulus gas interface is also regular. It can be seen that oxide defects (like oxide loss or broken oxide) are smaller than half the oxide thickness and that the oxide appearance is adherent, and compact.

b. O*xide thickness*

Figure 12 plots the axial profile of the average oxide thickness of the external surface for A-14 and L-12 pressure tubes. The oxide thickness at 0.3 m location from the inlet of PT L-12 was not measured. This Figure indicates that the oxide thickness increases slowly with the distance from the inlet end of the tube. The thickness varies between 2 to 5 μm for PT A-14 and between 2 to 3.5 μm for PT L-12. These values are similar to those reported by Warr et al [12] for the outside surface oxide of pressure tubes removed from CANDUs reactors.

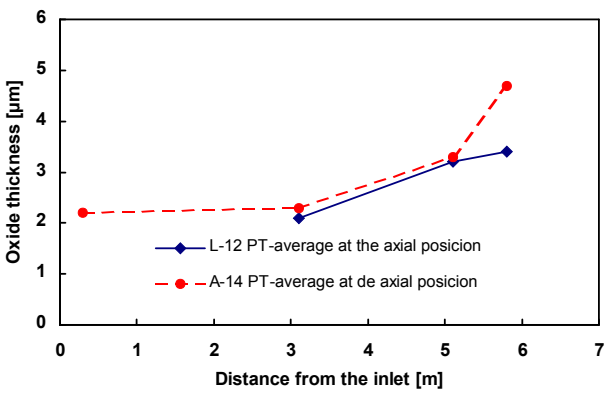

Fig. 12. Axial profile of the outside oxide thickness of PT A-14 and PT L-12.

Figure 13 plots the axial profile of the average oxide thickness at 3, 6, 9 and 12 o'clock positions of the internal surface for A-14 pressure tube and also depicts the average oxide thickness for each axial position. Figure 13 shows the same for L-12 pressure tube. These Figures indicate that the oxide thickness increases with the distance from the inlet end of the tube. As expected, the oxide thickens with increasing the coolant temperature along the tube. In the first two axial locations, the oxide thickness changes only slightly with changing the o'clock position, while the oxide thickness at 12 o'clock position is smaller in the last two axial locations. Warr et al. [12] reported similar oxide thickness differences at 6 and 12 o'clock positions for some pressure tubes that were in service during 10.3 EFPY in Pickering 3 NPP. These authors indicated that the greater oxide thickness found at 6 o'clock position should be associated with the higher temperature in this position compared with that at 12 o'clock position.

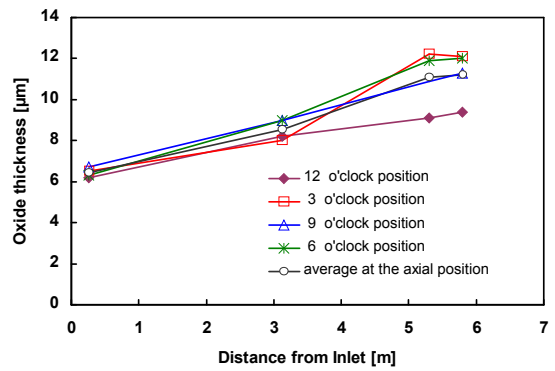

Fig. 13. Axial profile of the internal oxide thickness at 12, 3, 9 and 6 o'clock position and the average in axial location of PT A-14.

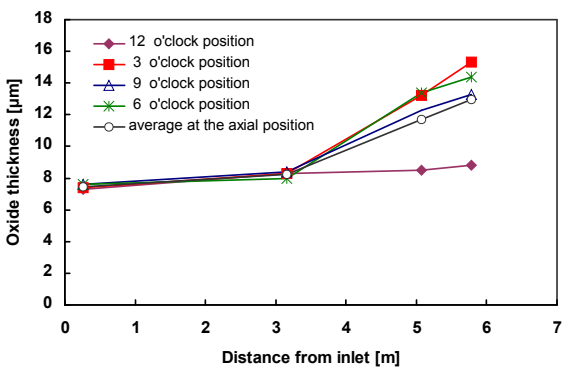

Fig. 14. Axial profile of the internal oxide thickness at 12, 3, 9 and 6 o'clock position and the average in axial location of PT L-12.

The oxide thickness of A-14 tube varies along it approximately between 6 to 12 μm and its average oxide thickness is 11 μm at 5.8 m axial location: In L-12 tube the oxide thickness varies approximately between 7 to 15 μm along it and its average oxide thickness is 13 μm at 5.8 m axial position. As the pressure tubes operated during 9.9 EFPY, the average corrosion rate was 1.2 and 1.5 μm/EFPY respectively. These values of corrosion rates are within the range of the values reported by Warr et al [17] for pressure tubes removed from Bruce A and other CANDUs 6 reactors.

The fuel channels A-14 and L-12 have a very different location when the neutron flux is considered. The fuel channel L-12 is a central one and consequently it is located in a zone of a higher fast neutron flux (E>1 Mev), than the fuel channel A-14 that is a peripheric one, so it works in a lower fast neutron flux zone. Figure 1 plotted the axial profile of fast neutron flux for both pressure tubes; showing that the fast neutron flux for fuel channel L-12 is higher than the double of the fuel channel A-14. The axial profile of temperature in the PHTS (Primary Heat Transport System) for both fuel channels was plotted in Figure 2. The last Figure shows that the temperature difference between both channels is not significant, particularly in the zones where the samples were cut out.

The range of oxide thicknesses of the inside surface at different axial locations for both tubes is compared in Figure 15. This Figure shows that the range of oxide thicknesses is similar for both tubes and the maximum thickness is slightly greater for the PT L-12 at 5 - 6 m location from the inlet of the PT.

These results should indicate a weak dependence of the corrosion rate with the fast neutron flux for this range of neutron flux and for the residence time of the tubes in the reactor. Warr et al. [17] have also indicated a weak dependence of the corrosion rate with the fast neutron flux.

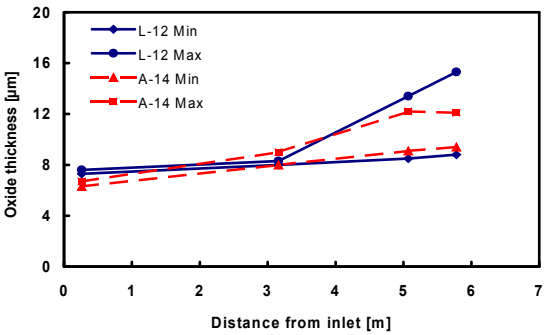

Fig. 15. Comparison of the range of oxide thicknesses of the inside surfaces for A-14 and L-12 PTs

Corrosion behavior of samples inserted in C.N. Embalse autoclaves

The primary heat transport system (PHTS) of Embalse NPP has two separate heat transport circuits, each one with two steam generators (SG) of the recirculating type. The system is provided with four in-line autoclaves, located out of the core in the primary coolant system, that are used to measure corrosion at outlet and inlet SG conditions (about 265 and 310°C). The coolant is lithiated heavy water, $pH_{25°C}$ = 10.2 - 10.4, hydrogen content 3-10 cm^3/kg D_2O [13,16,18]. Different structural material have been introduced in these autoclaves since 1983, coupons of Zr-2.5 Nb machined from non-irradiated TPs were included [13,18]. The long-term studies of these materials were carried out during more than 3400 EFPD of the plant service. Figure 15 depicts the oxidation kinetics of Zr-2.5Nb of pressure tubes samples exposed during 3400 EFPD (equivalent to 9.4 EFPY) in the two autoclaves that are at around 310°C in the two loops. This Figure also shows that the oxide thicknesses of the autoclave samples are similar to those of the PTs samples at 5.8 m axial location from the inlet of the tube after 9.9 EFPY.

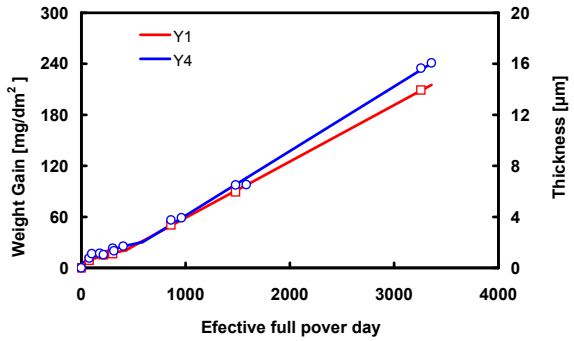

Fig. 15. Kinetics corrosion of Zr-2.5Nb samples cut from an unirradiated PT and exposed to the PHTS of Embalse NPP autoclaves.

Table II summarizes and compares the post-transition corrosion rates of the autoclave samples (that are at the outlet of the reactor) with the average corrosion rate at 5.8 m axial location of both PTs. The post transition corrosion rate values of the samples inserted in the CNE autoclaves are within the range of the values reported by Warr et al. [17] for off-cut samples also oxidized at 310°C.

Table II. Comparison of the corrosion rate of samples with and without neutron flux

Pressure Tube	Maximum Corrosion Rate (µm/EFPY)	Autoclave T ~ 310ºC	Post-transition corrosion rate (µm/EFPY)
A-14	1.2 ± 0.2	Y1	1.6 ± 0.2
L-12	1.5 ± 0.3	Y4	1.8 ± 0.2

These results indicate a similar corrosion behaviour in-pile and out-of pile of Zr-2.5Nb of pressure tube material up to the time of testing in the primary coolant. Warr et al. [17] reported similar results when they compared the post-transition corrosion rates of the off-cuts (material taken from the same PT before its installation in the Plant) tested at 310°C in autoclaves with the corrosion rates measured at the outlet coolant of pressure tubes of CANDU 600 and in Bruce NPP.

CONCLUSIONS

- SEM and EDS techniques have shown their usefulness to study relevant technical applications like those shown in this work in Nuclear Power Plants. Using them, we could determine the following points.
- The inside surface oxides of samples analysed from A-14 and L-12 pressure tubes were uniform, dull and black with a typical morphology reported for tubes removed from other CANDU reactors. In some zones, near the coolant outlet where some spalling was observed, the remaining oxide thickness was sufficient to assure the protective character of the oxide.
- The oxide of the inside surface varies between 6 to 14 µm in PT L-14 and between 7 to 15 µm in PT L-12. The average corrosion rates at 5.8 m location from the inlet of the tubes were 1.2 and 1.5 µm/EFPY in PTs A-14 and L-12 respectively. These corrosion rates values are within the range of those reported for other pressure tubes removed from Bruce A and other CANDUs 6 reactors.
- The outside surface oxide of all the samples studied in both pressure tubes was black, compact and more reflective than that of the inside surface. The oxide replicates the original outside tube surface and the thickness varies between 2 to 5 µm in A-14 and 2 to 3.5 µm for L-12.
- The post-transition corrosion rate of the Zr-2.5Nb coupons of pressure tubes inserted in the hotter (310°C) C.N. Embalse autoclaves is nearly equal to the average corrosion rate of the inside surfaces located at around 5 to 5.8 m from the inlet of the PTs. This result could be explained by the overlapping of the decrease of the corrosion rate

induced by the fluence effect on the material and the increase of this corrosion rate due to the effect of the oxide thickness and the fast neutron flux.

ACKNOWLEDGEMENT

Work was supported by Comisión Nacional de Energía Atómica (CNEA) and partially by NASA (Nucleoeléctrica Argentina Sociedad Anónima).

REFERENCES

[1] Olmedo, A.M, Miyagusuku, M, Rosenbusch, M, Bordoni, R. (2010) "Aplicaciones de microscopía de barrido y espectroscopía dispersiva de rayos X en el ámbito de Centrales Nucleares" *Acta Microscopica* 19, Supp.A: 32-43.

[2] Urbanic, V.F., Gilbert, R.W. (1990) "Effect of Microstructure on the Corrosion of Zr-2.5Nb Alloy", Fundamental Aspects of Corrosion on Zirconium Base Alloys in Water Reactor Environments, *International Atomic Energy Agency (IAEA)*, Vienna (Ed.1990): 262-272.

[3] Mc Dougall, G.M., Urbanic, V.F. (2002) "The Influence of Material Variables on Corrosion and Deuterium Uptake of Zr-2.5Nb Alloy During Irradiation", *Zirconium in the Nuclear Industry, Thirteenth International Symposium*. ASTM STP 1423:247-273.

[4] McDougall, G.M. Urbanic, V.F., Aarrestad, O. (2000) "Studies of Zirconium Alloy Corrosion and Hydrogen Uptake During Irradiation", *Zirconium in the Nuclear Industry, Twelfth International Symposium*. ASTM STP 1354: 756-772.

[5] Bahurmuz, A.A., Muir I.J, Urbanic, V.F. (2006) "Predicting Oxidation and Deuterium Ingress for Zr-2.5Nb CANDU Pressure Tubes", *Fourteenth International Symposium of Zirconium in the Nuclear Industry*: ASTM STP 1467: 547-561.

[6] Griffiths, M, Winegar, J.E., Buyers, A. (2008) "The Transformation Behaviour of the Beta Phase in Zr-2.5 wt % Nb Pressure Tubes", *Journal of Nuclear Materials* 383: 28-33.

[7] Maroto, A.J.G., Bordoni, R., Villegas, .M., Olmedo, A.M., Blesa, M.A, Iglesias, A., Koenig, P. (1996) "Growth and Characterization of Oxide Layers on Zirconium Alloys", *Journal of Nuclear Materials* 229: 79-92.

[8] Jaime Solís, F., Bordoni, R., Olmedo, A.M., Villegas, M., Miyagusuku, M. (2001) "Comportamiento a la Corrosión Acuosa del Zr-1Nb y Zr-20Nb con Diferentes Tratamientos Térmicos, *Actas de la XXVIII Reunión Anual de la Asociación Argentina de Tecnología Nuclear*, Buenos Aires, noviembre 2001.

[9] Jaime Solís, F., Bordoni, R., Olmedo, A. M., Villegas, M., Miyagusuku, M. (2001) "Comportamiento a la Corrosión Acuosa del Zr-2.5Nb con Diferentes Tratamientos Termicos", *Actas de la XXVIII Reunión Anual de la Asociación Argentina de Tecnología Nuclear*, Buenos Aires, noviembre 2001.

[10] Urbanic, V.F., Griffiths, M. (1996) "Corrosion Response of Preirradiated Zr-2.5Nb Pressure Tube Materials", Effects of radiation on Materials, *11th International Symposium in the Nuclear Industry*,, ASTM STP 1270: 1088.

[11] Urbanic, V.F.,Griffiths, M (2000) "Microstructural Aspects of Corrosion and Hydrogen Ingress in Zr-2.5Nb", *Twelfth International Symposium Zirconium in the Nuclear Industry*, ASTM STP 1354: 641-657.

[12] Warr, B.D., Van Der Heide, P.A.W., Maguire, M.A. (1996) "Oxide Characteristics and Corrosion and Hydrogen Uptake in Zr-2.5Nb CANDU Pressure Tubes", *Proc. of the 11th Zirconium in the Nuclear Industry*, ASTM STP 1295: 265-291.

[13] Olmedo, A. M., Bordoni, R:, Miyagusuku, M, Chocrón, M, Fernández, Quinteros D., Ovando, L., Sainz, R. (2008) "Corrosion Monitoring of Structural Materials in the Primary Coolant Circuit Of Embalse N.P.P", *Proceedings of the International Conference on Water Chemistry of Nuclear Reactor Systems* VGB NPC'08, Sep .2008, Berlin, Germany, P2-08.

[14] Bossis, P., Leliévre, G., Barberis, P., Iltis, X., Lefebvre, F. (2000) "Multiscale Characterization of the Metal-Oxide Interface of Zirconium Alloys", *Proc. of the 12th Zirconium in the Nuclear Industry*, ASTM STP 1354: 918-945.

[15] Bossis, P., Pêcheur, D., Hanifi, K., Thomazet, J., Blatt, M. (2006) "Comparison of the High Burn-Up Corrosion on M5 and Low Tin Zircaloy 4", *14th International Symposium of Zirconium in the Nuclear Industry*, ASTM STP 1467: 494-525.

[16] Maroto, A.J.G., Bordoni, R, Olmedo, A.M., Villegas, M., Chocrón, M., Szpunar, J (1999) "Corrosion Behaviour and Deposition of Crud on Zr-Alloys", *Proceedings of a Technical Committee meeting "Water Chemistry and Corrosion Control of Cladding and Primary Circuit Components"* IAEA TECDOC-1128: 163-178.

[17] Warr, B.D., Perovic, V., Lin, Y.P., Wallace, A.C. (2002) "Role of Microchemistry and Microstructure on Variability in Corrosion and Deuterium of Zr-2.5Nb Pressure Tube Material", *Proc. of the 13th Zirconium in the Nuclear Industry*, ASTM STP 1423: 313-338.

[18] Villegas, M. Olmedo, A.M., Bordoni, R., Alvarez, M.G., Miyagusuku, M., Saínz, R. (1995) "Surveillance Program of Corrosion-related Degradation of *Structural Materials in Primary Reactor Coolant", IAEA Specialist Meeting on the "Effectiveness of Methods for the Detection and Monitoring of Age Related Degradation in Nuclear Power Plants"*, San Carlos de Bariloche, Argentina October 1995.